Chemical Physics 369 (2010) 27–36

Contents lists available at ScienceDirect

Chemical Physics

journal homepage: www.elsevier.com/locate/chemphys

Photo-degradation behaviour of roseoflavin in some aqueous solutions

A. Tyagi [a], A. Penzkofer [a,*], T. Mathes [b], P. Hegemann [b]

[a] Institut II – Experimentelle und Angewandte Physik, Universität Regensburg, Universitätsstraße 31, D-93053 Regensburg, Germany
[b] Institut für Biologie/Experimentelle Biophysik, Humboldt Universität zu Berlin, Invalidenstraße 42, D-10115 Berlin, Germany

ARTICLE INFO

Article history:
Received 23 December 2009
In final form 3 February 2010
Available online 10 February 2010

Keywords:
Roseoflavin
8-Methylamino-riboflavin
Absorption spectroscopy
Fluorescence spectroscopy
Photo-induced charge-transfer
Photo-degradation
Triplet–singlet excitation transfer

ABSTRACT

An absorption and emission spectroscopic characterization of roseoflavin (8-dimethylamino-8-demethyl-riboflavin, RoF) in aqueous solutions was carried out. The studies were concentrated on roseoflavin in pH 8 phosphate buffer. Absorption cross-section spectra, fluorescence excitation spectra, fluorescence quantum distributions, fluorescence quantum yields and fluorescence lifetimes were determined. The fluorescence of RoF is quenched by photo-induced intra-molecular charge-transfer at room temperature. The photo-degradation of RoF in un-buffered water, in Tris–HCl buffer, and in phosphate buffer was studied. Phosphate buffer and to a smaller extent Tris buffer catalyse the RoF photo-degradation. Photo-excitation of the primary photoproduct, 8-methylamino-riboflavin (8-MNH-RF), enhanced the RoF degradation by triplet 8-MNH-RF – singlet RoF excitation transfer with subsequent triplet-state RoF degradation.

1. Introduction

Roseoflavin (8-dimethylamino-8-demethyl-D-riboflavin, RoF) is a riboflavin derivative with modified absorption and emission spectroscopic behaviour [1] (first absorption band red-shifted with larger absorption strength than riboflavin, fluorescence emission very weak). The biological function of roseoflavin is different from that of riboflavin (vitamin B_2) [2]. It acts as an antibiotic [3] and vitamin B_2 antagonist [4]. Substitution of riboflavin, flavin mononucleotide (FMN) and flavin adenine dinucleotide (FAD) by RoF and its counterparts RoFMN and RoFAD in flavoproteins during protein expression has been achieved ([5] and references therein). In most cases the biological cofactor action was lost or strongly reduced by the cofactor exchange [6–9].

The absorption behaviour of roseoflavin in several solvents was reported in [1,3,7,10–16]. The fluorescence behaviour of roseoflavin was studied in [11,13,16,17]. The photo-stability of roseoflavin in aqueous solution under different pH conditions was studied in [1,11,17,18].

In this paper, the absorption and emission spectroscopic behaviour of roseoflavin was mainly studied in aqueous pH 8 10 mM sodium phosphate buffer (abbreviated by NaP_i, composition: 0.68 mM $Na^+H_2PO_4^-$, 9.32 mM $Na_2{}^{2+}HPO_4^{2-}$, and 10 mM NaCl). Photo-degradation studies were carried out on roseoflavin in pH 8 phosphate and Tris–HCl buffers (Tris = $(CH_2CH_2OH)_3C–NH_2$) of different molarity, in pH 10 10 mM phosphate buffer, and in neutral un-buffered water. The photo-stability of RoF was found to be highest in pure water, reduced by Tris–HCl buffer, and more strongly reduced by phosphate buffer. The photo-degradation was found to be enhanced by the intermediate photoproduct 8-methylamino-riboflavin (8-MNH-RF).

Bi-anionic phosphate (HPO_4^{2-}) and sulphate (SO_4^{2-}) catalysed photo-degradation of riboflavin and FMN is well established in the literature [19–22]. The bi-anionic catalytic conversion of riboflavin to 2′,9-cyclo-dehydro-riboflavin was identified [20].

The structural formulae of roseoflavin (RoF) and of derivative classes are displayed in Fig. 1.

2. Experimental

The dye RoF was bought from Toronto Research Chemicals Inc., North York, Canada. The specified purity was >97%. It was dissolved in aqueous solutions. If not stated different experiments were carried out at room temperature under aerobic conditions.

Transmissions were measured with a commercial spectrophotometer (Cary 50 from Varian), fluorescence emission and fluorescence excitation spectra were recorded with a commercial spectrofluorimeter (Cary Eclipse from Varian).

Fluorescence lifetime measurements were performed with second harmonic pulses of a mode-locked titanium–sapphire laser system (Hurricane from Spectra Physics) and an ultrafast streak-camera (type C1587 temporal disperser with M1952 high speed streak unit from Hamamatsu) [16]. Picosecond excitation pulses at 456 nm were generated by stimulated Raman scattering of second harmonic pulses (wavelength 402 nm, duration 4 ps) of

* Corresponding author. Tel.: +49 941 943 2107; fax: +49 941 943 2754.
E-mail address: alfons.penzkofer@physik.uni-regensburg.de (A. Penzkofer).

0301-0104/$ - see front matter © 2010 Elsevier B.V. All rights reserved.
doi:10.1016/j.chemphys.2010.02.004

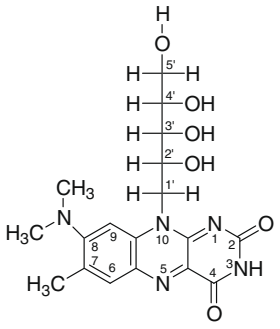

Roseoflavin (RoF)

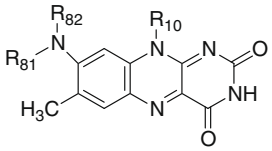

8-amino-flavin derivatives (AF)

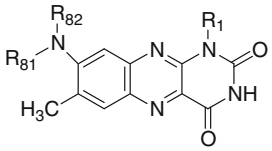

8-amino-lumichrome derivatives (ALC)

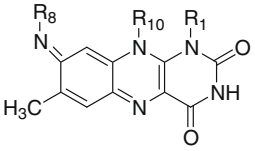

8-amino-quinone-flavin derivatives (AQF)

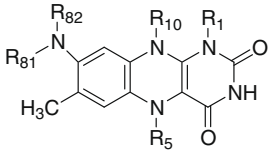

Fully reduced 8-amino-flavin derivatives (AF_{red2})

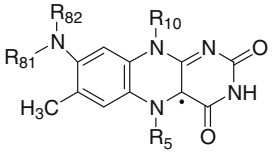

Semi-reduced 8-amino- C4a-flavin derivatives (C4a-AF_{red1})

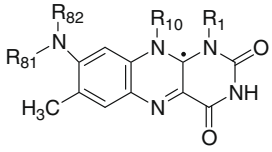

Semi-reduced 8-amino- C10a-flavin derivatives (C10a-AF_{red1})

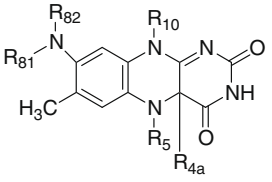

8-amino- C4a-flavin adducts

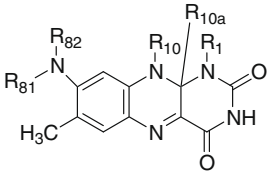

8-amino- C10a-flavin adducts

Fig. 1. Structural formulae of roseoflavin (RoF), 8-amino-flavin derivatives (AF), 8-amino-lumichrome derivatives (ALC), 8-amino-quinone-flavin derivatives (AQF), fully reduced 8-amino-flavin derivatives (AF_{red2}), semi-reduced 8-amino-C4a-flavin derivatives, semi-reduced 8-amino-C10a-flavin derivatives, 8-amino-C4a-flavin adducts, 8-amino-C10a-flavin adducts. Abbreviations: R_{81}, R_{82} = CH_3, H. R_{10} = ribityl, C2′-keto-ribityl, C4′-keto-ribityl, CH_2CHO. R_1 = CH_3, H, OH. R_5 = H, OH. R_{4a}, R_{10a} = H, OH.

the Ti:sapphire laser system in ethanol (Stokes shift 2928 cm^{-1}) [8] using a Raman generator–amplifier arrangement [9] with two 5 cm cells in series (distance between cells approximately 10 cm for divergence reduction). Part of the fluorescence lifetime measurements were also carried out with a mode-locked picosecond Nd–glass laser system [23] (second harmonic pulses at 527 nm of 6 ps duration).

The photo-degradation was studied by sample excitation with a high-pressure mercury lamp in combination with interference filters. Part of the photo-degradation studies were carried out by excitation with second harmonic light of a small cw Nd:YAG laser (wavelength 532 nm, power 4.5 mW).

3. Results

3.1. Absorption and fluorescence characterization

The absorption cross-section spectrum of roseoflavin (RoF) in aqueous pH 8 10 mM NaP_i buffer is shown in Fig. 2. It fully agrees with the absorption cross-section spectrum of RoF in aqueous pH 8 Tris–HCl buffer [16]. The S_0–S_1 absorption strength is $\bar{\sigma}_a = \int_{\lambda_u}^{\infty}[\sigma_a(\lambda)/\lambda]\,d\lambda = (2.3 \pm 0.2) \times 10^{-17}$ cm^2 (upper wavelength position set to 420 nm). Included in Fig. 2 are the absorption cross-section spectra of 8-MNH-RF in neutral aqueous solution (from [24]) and of 8-amino-riboflavin (8-NH_2-RF) in aqueous pH 8 buffer (from [17]).

Fluorescence quantum distributions, $E_F(\lambda)$, of RoF in pH 8 phosphate buffer for some excitation wavelengths are shown in Fig. 3. For $\lambda_{F,exc}$ = 450 nm the fluorescence quantum yield is largest due to fluorescence contribution from riboflavin contamination (fluorescence quantum yield of riboflavin at pH 8 is 0.26 [25]). The presence of a mole fraction of x_{RF} = 0.0025 is calculated. At $\lambda_{F,exc}$ = 540 nm the fluorescence quantum distribution is dominantly determined by RoF emission. At $\lambda_{F,exc}$ = 505 nm $E_F(\lambda)$ is dominated by the degradation product 8-MNH-RF which is already present in a small amount.

The radiative lifetime of RoF is determined from the S_0–S_1 absorption strength $\bar{\sigma}_a$ and the mean fluorescence wavelength, $\bar{\lambda}_F = [\int E_F(\lambda)\lambda^3 d\lambda / \int E_F(\lambda) d\lambda]^{1/3}$, by the Strickler–Berg formula [26–28],

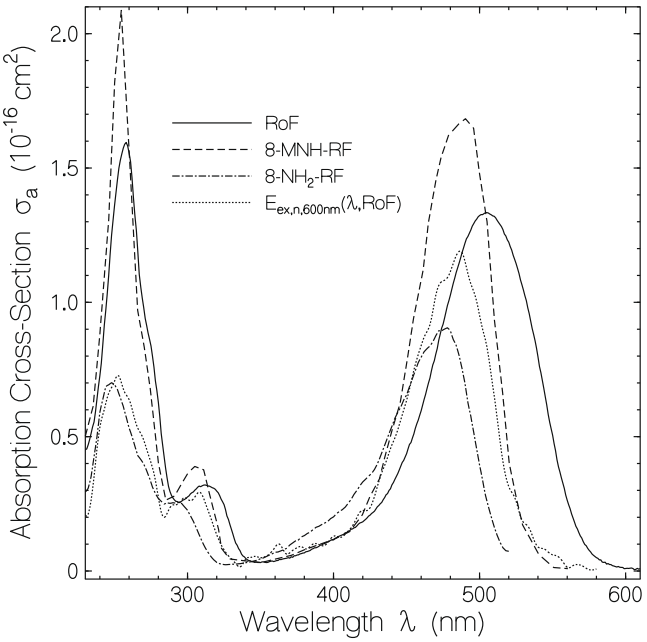

Fig. 2. Absorption cross-section spectra, $\sigma_a(\lambda)$, of RoF in aqueous pH 8 buffer (this work), 8-MNH-RF in neutral aqueous solution (from [24]), and of 8-NH_2-RF in Millipore water (from [37]). The fluorescence excitation spectrum of RoF is included (detection wavelength: 600 nm, normalized to absorption spectrum at 488 nm).

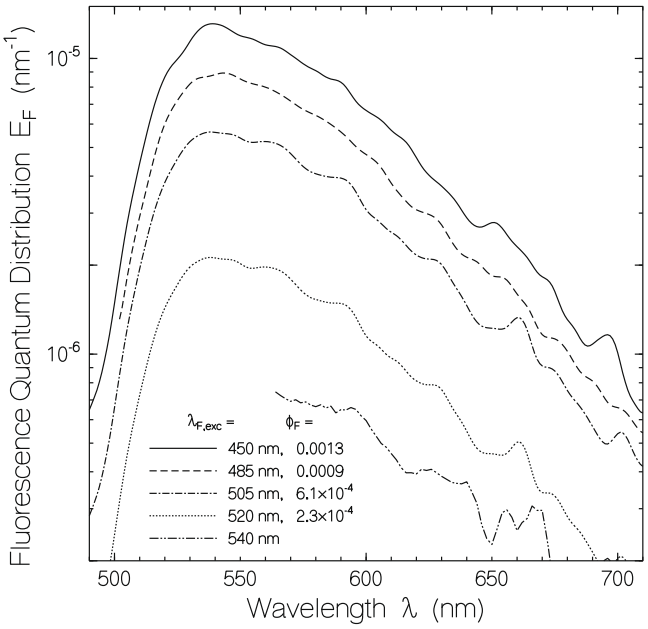

Fig. 3. Fluorescence quantum distributions, $E_F(\lambda)$, of RoF sample in pH 8 10 mM NaP_i buffer at different fluorescence excitation wavelengths, $\lambda_{F,exc}$. The obtained fluorescence quantum yields, ϕ_F, are listed in the figure. Differences are due to the presence of trace amounts of riboflavin and 8-MNH-RF.

$$\tau_{rad} = \frac{n_A \bar{\lambda}_F^3}{8\pi c_0 n_F^3 \bar{\sigma}_a}, \tag{1}$$

where n_A and n_F are the average refractive indices in the S_0–S_1 absorption and emission region ($n_A \approx n_F \approx 1.33$), respectively, and c_0 is the speed of light in vacuum. The result is $\tau_{rad} = 6.5 \pm 0.4$ ns.

Two temporal fluorescence traces are shown in Fig. 4a and b for RoF in pH 8 10 mM NaP_i buffer. The traces were obtained by sample excitation at 456 nm with light pulses of 4 ps duration and

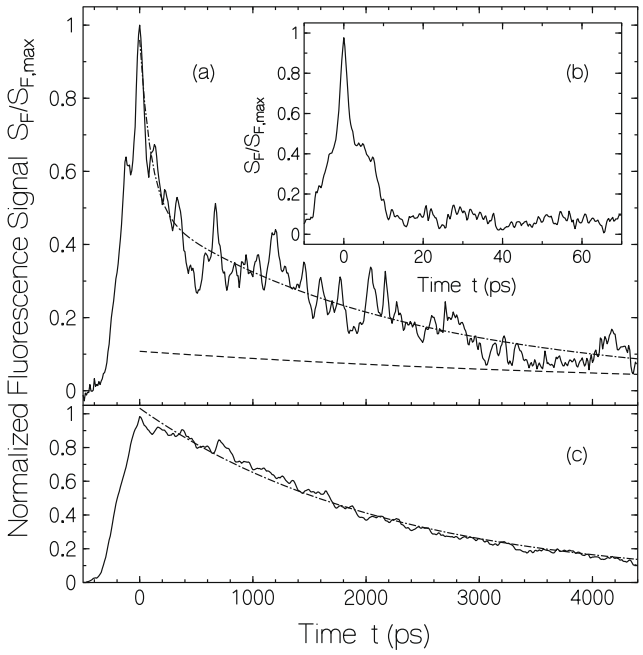

Fig. 4. Temporal fluorescence traces of RoF in aqueous pH 8 10 mM NaP_i buffer. Fluorescence excitation occurred at 456 nm with light pulses of 4 ps duration. Curves were measured with a streak-camera. (a) Unexposed sample, streak speed of 10 ps/pixel. Dashed curve: calculated riboflavin contribution ($S_F/S_{F,max} = 0.10^8\exp(-t/5\text{ ns})$). Dash-dotted curve: nonlinear regression fit ($S_F/S_{F,max} = 0.10^8\exp(-t/5\text{ ns}) + 0.48\exp(-t/0.1\text{ ns}) + 0.412\exp(-t/1.98\text{ ns})$). (b) Unexposed sample, streak speed of 0.33 ps/pixel. (c) Sample exposed in wavelength range from 425 nm to 503 nm with intensity of 0.085 W cm^{-2} for 65 min. Trace is caused by fluorescence decay of 8-MNH-RF. Dash-doted curve: single-exponential fit with $\tau_F = 2.18$ ns.

fluorescence signal detection with our streak-camera. The trace in the main frame (a) was measured with a streak speed of 10 ps/pixel, and the trace in the small frame (b) was recorded with a streak speed of 0.33 ps/pixel. In the main frame the riboflavin contribution to the fluorescence signal is indicated by the dashed line. The short peaks at time $t = 0$ in Fig. 4a and b are not time-resolved because of streak speed limitations. The dash-dotted curve in Fig. 4a shows a three-exponential regression fit,

$$S_F(t)/S_F(0) = x_1 \exp\left(-t/\tau'_{F,1}\right) + x_2 \exp\left(-t/\tau_{F,2}\right) + x_3 \times \exp\left(-t/\tau_{F,3}\right), \tag{2a}$$

with $x_1 = 0.48$, $\tau'_{F,1} = 100$ ps, $x_2 = 0.412$, $\tau_{F,2} = 1.97$ ns, $x_3 = 0.108$, $\tau_{F,3} = 5$ ns. The true fluorescence lifetime of the short component is extracted by involving the fluorescence quantum yield [16]. The total fluorescence quantum yield is

$$\phi_F = \phi_{F,1} + \phi_{F,2} + \phi_{F,3}, \tag{2b}$$

with a value of $\phi_F(456\text{ nm}) = 0.0012$ (see Fig. 3). The fluorescence quantum yield of the short component is

$$\phi_{F,1} = \frac{x_1 \tau'_{F,1}}{x_1 \tau'_{F,1} + x_2 \tau_{F,2} + x_3 \tau_{F,3}} \phi_F, \tag{2c}$$

giving $\phi_{F,1} = 6.7 \times 10^{-5}$. The fluorescence lifetime is

$$\tau_{F,1} = \phi_{F,1} \tau_{rad}, \tag{2d}$$

which gives $\tau_{F,1} = 0.44 \pm 0.05$ ps. The component with $\tau_{F,1} = 0.44$ ps lifetime is attributed to locally excited direct fluorescence emission of RoF. This short locally excited-state lifetime is thought to be determined by efficient twisted intra-molecular charge-transfer (TICT) [16]. The slow component with $\tau_{F,2} = 1.97$ ns is attributed

dominantly to the presence of a small fraction of 8-MNH-RF which is a photo-degradation product of RoF (some time-delayed locally excited-state fluorescence emission of RoF may contribute [16], but it cannot be resolved from the dominant 8-MNH-RF contribution). The component with $\tau_{F,3} = 5$ ns belongs to the riboflavin contamination.

A normalized fluorescence excitation spectrum of our RoF in pH 8 NaP_i buffer is included in Fig. 2. The fluorescence was detected at $\lambda_{det} = 600$ nm and it is normalized to the absorption cross-section spectrum of RoF at 488 nm according to $E_{ex,n}(\lambda) = [E_{ex,600\,nm}(\lambda)/E_{ex,600\,nm}(488\,nm)]\sigma_a(488\,nm)$. The shape of the presented excitation spectrum does not fit to the shape of the RoF absorption cross-section spectrum. It better fits to the absorption cross-section spectrum of 8-MNH-RF. This finding clearly shows that the small fraction of present 8-MNH-RF dominates the fluorescence emission since RoF is extremely weak emitting. In the UV spectral range below 320 nm, the excitation spectrum becomes smaller than the absorption cross-section spectrum indicating that the higher excited states only partly relax via the first exited state (other decay channels are present, violation of Vavilov–Kasha rule of excitation wavelength independent fluorescence emission [29,30]).

3.2. Photo-degradation studies

The photo-degradation behaviour of RoF was studied by long-time sample exposure and measurement of absorption spectra, fluorescence emission spectra, and fluorescence excitation spectra at certain time points.

In Fig. 5a, the development of the absorption coefficient spectra of 0.047 mM RoF in pH 8 10 mM NaP_i buffer is shown. The sample was excited at $\lambda_{exc} = 425$–503 nm with an intensity of $I_{exc} = 0.085$ W cm^2. The original absorption band of RoF peaking at 504 nm transforms to an absorption band peaking at 488 nm (formation of 8-MNH-RF). The change starts slowly within the first hour, then speeds up, and is roughly completed after 2 h of exposure. The formed absorption band around 488 nm decreases with continued light exposure. A spectral shoulder around 470 nm develops (likely formation and decay of 8-amino-riboflavin, 8-NH_2-RF). A spectral structure forms out in the 340 nm to 420 nm region (indication of formation of 8-dimethylamino-lumichrome, 8-methylamino-lumichrome, and 8-amino-lumichrome, see Fig. 1 for structural formulae). An absorption tail remains in the 540–590 nm range (roseoflavin quinonoid structure formation by photo-induced methyl-transfer from the 8-dimethylamino group to the N1 position, see Fig. 1 for structural formulae). The photo-degradation strongly reduces the absorption strength of the first absorption band in the 400 to 550 nm region indicating dominant roseoflavin reduction (fully reduced 8-amino-flavin structure formation by hydration, hydroxylation or methylation at N5 and N1 positions, for structural formulae see Fig. 1). In Fig. 5b, the absorption spectra of Fig. 5a are shown after approximate subtraction of the remaining RoF contribution. The initial increase and later decrease of the 8-MNH-RF contribution is clearly seen. Some indication of build-up and decrease of 8-NH_2-RF is found (has peak absorption at about 478 nm, see Fig. 2). The formation of a quinonoid structure is revealed by the build-up of an absorption band around 560 nm. Some 8-amino-C4a-flavin-semiquinone or 8-amino-C10a-flavin-semiquinone formation with absorption around 560 nm is thought to be unlikely because of expected low photostability. The absorption structure in the 340–420 nm region shows the presence of an 8-amino-lumichrome component. The presence of small amounts of 8-amino-riboflavin-C4a-adducts or 8-amino-riboflavin-C10a-adducts with H, OH, CH_3 as adducts cannot be excluded.

The development of the absorption coefficients of RoF in pH 8 10 mM NaP_i at the selected wavelengths $\lambda_{pr} = 540$ nm (only RoF absorption) and 488 nm (peak absorption of 8-MNH-RF) versus the exposed incident energy density is shown by the line-connected circles in Fig. 6a and b, respectively (data taken from

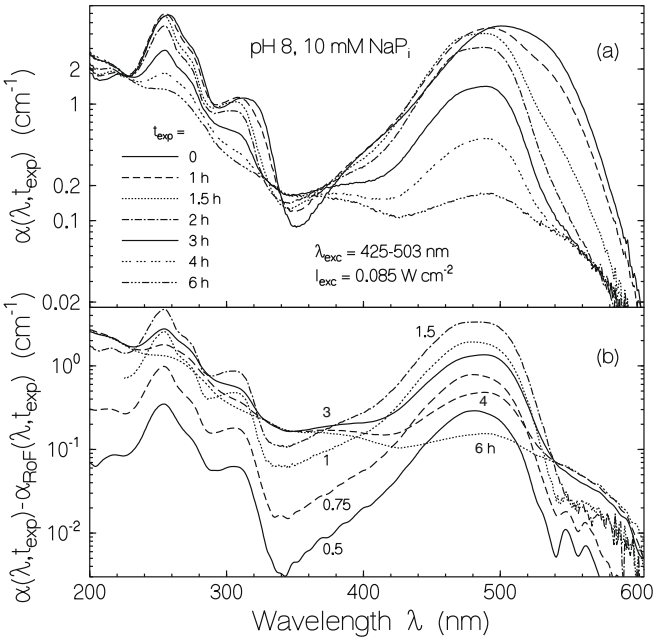

Fig. 5. Absorption spectra development due to blue-light exposure. Excitation wavelength $\lambda_{exc} = 425$–503 nm. Excitation intensity $I_{exc} = 0.085$ W cm^{-2}. Exposure times, t_{exp}, are indicated in the sub-figures. (a) Measured absorption coefficient spectra at different times of exposure. (b) Obtained absorption coefficient spectra after subtraction of remaining RoF contribution.

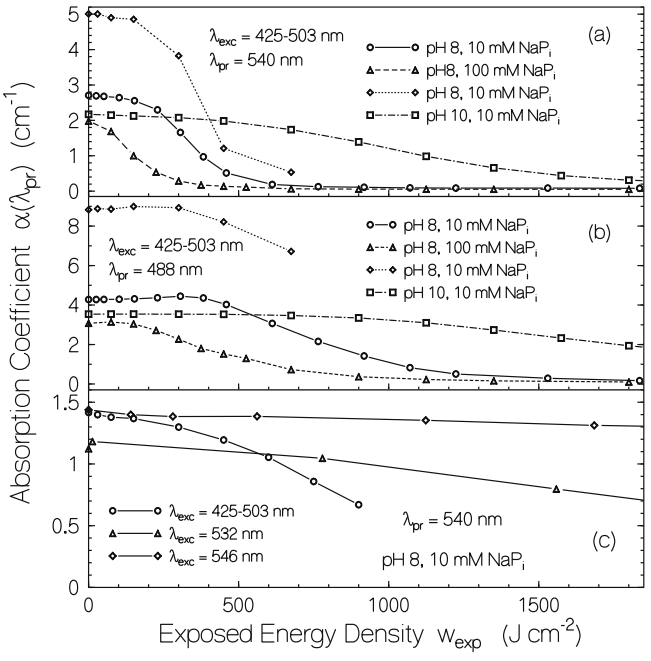

Fig. 6. Development of absorption coefficients of RoF in phosphate buffer versus exposed excitation energy density w_{exp}. (a) Excitation in the wavelength range $\lambda_{exc} = 425$–503 nm and absorption probing at $\lambda_{pr} = 540$ nm (only absorption of RoF). (b) Excitation in the wavelength range $\lambda_{exc} = 425$–503 nm and absorption probing at $\lambda_{pr} = 488$ nm (absorption peak of 8-MNH-RF). (c) Excitation at different wavelengths ($\lambda_{exc} = 425$–503 nm, $I_{exc} = 0.25$ W cm^{-2}; $\lambda_{exc} = 532$ nm, $I_{exc} = 0.22$ W cm^{-2}; $\lambda_{exc} = 546$ nm, $I_{exc} = 0.16$ W cm^{-2}) and absorption probing at $\lambda_{pr} = 540$ nm.

Fig. 5a, $w_{exp} = I_{exc} t_{exp}$). The trace for λ_{pr} = 540 nm shows the photo-degradation of RoF. It starts with low efficiency and then becomes rather effective. The absorption decrease levels off at high exposed energy density because of absorption of the formed 8-methylamino quinone flavin and fully reduced roseoflavin (RoF_{red2}). The trace for λ_{pr} = 488 nm shows the formation and decrease of 8-MNH-RF, likely with some contribution of 8-NH_2-RF formation and decay.

From the absorption decrease with light exposure quantum yields of photo-degradation, ϕ_D, may be determined. The quantum yield of photo-degradation, ϕ_D, is defined by

$$\phi_D(t_{exp}) = \frac{\delta N_D(t_{exp})}{\delta n_{ph,abs}(t_{exp})} = \frac{[\alpha_{pr}(t_{exp}+\delta t) - \alpha_{pr}(t_{exp})]/\sigma_{a,pr}}{\frac{I_{exc}\delta t}{h\nu_{exc}}\alpha_{exc}(t_{exp})}, \quad (3)$$

where δN_D is the number density of degraded molecules (unit cm^{-3}) in a time interval δt at t_{exp}, and $\delta n_{ph,abs}$ is the number density of absorbed photons (unit cm^{-3}) in the same time interval δt at t_{exp}. We estimate an initial quantum yield of photo-degradation of RoF from the initial absorption decrease at 540 nm (see Figs. 5 and 6a) of $\phi_{D,0}(RoF) \approx 1.15 \times 10^{-6}$. With time of exposure the quantum yield of photo-degradation increased. For t_{exp} = 75 min a value of $\phi_D(75\ min,\ RoF) \approx \phi_{D,max}(RoF) \approx 2.3 \times 10^{-5}$ is determined. The quantum yield of photo-degradation of the formed 8-MNH-RF is estimated from the absorption decrease at λ_{pr} = 488 nm for t_{exp} = 2.5 h (w_{exp} = 765 J cm^{-2}). A value of ϕ_D(2.5 h, 8-MNH-RF) $\approx 2 \times 10^{-5}$ is estimated.

In Fig. 7 the fluorescence development of 0.047 mM roseoflavin in 10 mM NaP_i pH 8 buffer due to light exposure at λ_{exc} = 425–503 nm with I_{exc} = 0.085 W cm^{-2} is shown. In part (a) the fluorescence was excited at $\lambda_{F,exc}$ = 470 nm. The fluorescence signal rises and decreases with the formation and degradation of 8-MNH-RF. It shifts a little bit to the blue side for $t_{exp} \geqslant 2$ h likely due to the formation and degradation of 8-NH_2-RF. In part (b) the fluorescence was excited at $\lambda_{F,exc}$ = 360 nm. The fluorescence signal in the 400–500 nm range belongs to 8-amino-lumichromes. The fluorescence band peaking in the 520–540 nm region belongs mainly to 8-MNH-RF and 8-NH_2-RF emission and resembles the 8-MNH-RF and 8-NH_2-RF build-up and decrease.

In Fig. 8, fluorescence excitation spectra are shown for the same experimental situation as in Figs. 5 and 7. The emission was detected at λ_{det} = 600 nm (a) and at λ_{det} = 450 nm (b). In part (a) the build-up and decay of the fluorescent photoproducts 8-MNH-RF and 8-NH_2-RF is manifested in the excitation spectrum development in the 420–520 nm range. Some formation of 8-amino-lumichromes is revealed by the excitation spectra shape changes in the 330–420 nm range. The 8-amino-lumichrome formation is more clearly seen in the excitation spectra development in part (b). The inset (c) shows the fluorescence excitation signal $E_{ex,450nm}$ (λ = 360 nm) as a function of exposure time. The signal (amino-lumichrome formation) rises during RoF degradation (t_{exp} < 3 h) and during 8-MNH-RF and 8-NH_2-RF degradation (t_{exp} > 1 h).

A temporal fluorescence trace measured on 0.047 mM roseoflavin in 10 mM NaP_i pH 8 buffer after 65 min of light exposure at λ_{exc} = 425–503 nm with I_{exc} = 0.085 W cm^{-2} is displayed in Fig. 4c (fluorescence creation with 4 ps laser pulse at 456 nm). It is fitted with a single-exponential decay function of time constant τ_F = 2.18 ns. It gives the fluorescence lifetime of 8-MNH-RF.

The absorption coefficient development at λ_{pr} = 540 nm (Fig. 6a) and λ_{pr} = 488 nm (Fig. 6b) versus exposed energy density was studied for different NaP_i buffer and RoF concentrations (seen by different initial absorption coefficients). Light excitation occurred in the wavelength range of 425–503 nm. The line-connected circle curves (0.047 mM RoF in 10 mM NaP_i pH 8 buffer) were alredy discussed above. The dashed-line-connected triangles belong to 100 mM NaP_i pH 8 buffer (sample temperature ϑ = 4 °C). The efficiency of photo-degradation increased with the phosphate buffer concentration (steeper initial absorption decrease at λ_{pr} = 540 nm). The dotted-line connected diamonds belong to higher concentrated RoF (C = 0.092 mM) in 10 mM NaP_i pH 8 buffer (ϑ = 4 °C). The initial

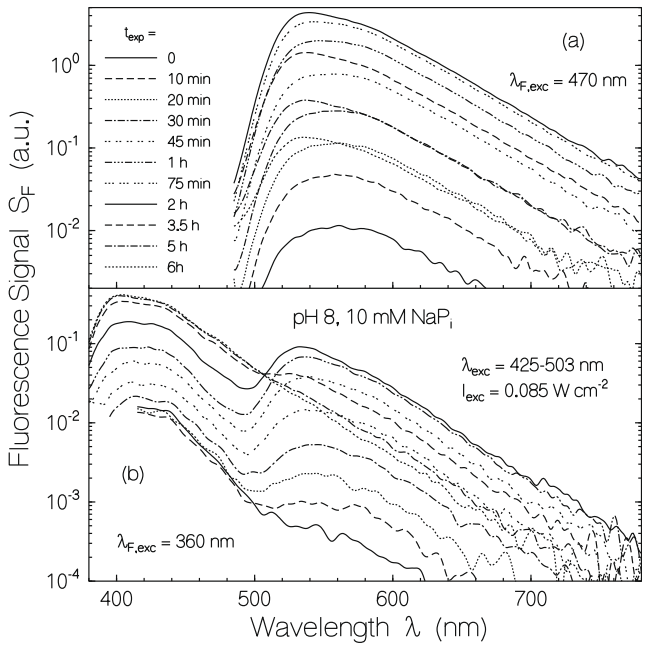

Fig. 7. Fluorescence-emission-spectra development of RoF im 10 mM NaP_i pH 8 buffer due to blue-light exposure (λ_{exc} = 425–503 nm, I_{exc} = 0.085 W cm^{-2}). Parameters are the same as in Fig. 5. (a) Fluorescence excitation at 470 nm (dominant emission from 8-MNH-RF and 8-NH_2-RF). (b) Fluorescence excitation at 360 nm (dominant short-wavelength emission from 8-dimethylamino-lumichrome, 8-methylamino-lumichrome, and 8-amino-lumichrome).

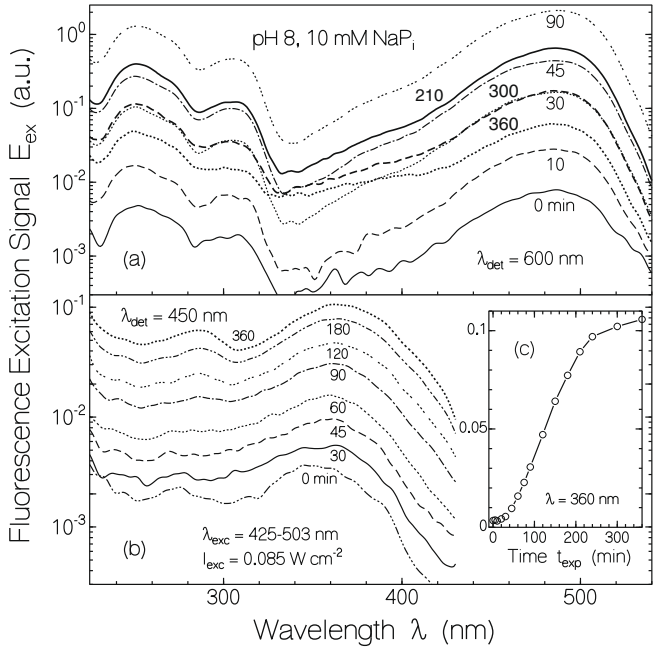

Fig. 8. Fluorescence excitation spectra development of RoF im 10 mM NaP_i pH 8 buffer due to blue-light exposure (λ_{exc} = 425–503 nm, I_{exc} = 0.085 W cm^{-2}). Parameters are the same as in Fig. 5. (a) Fluorescence detection at λ_{det} = 600 nm. The curves belong to indicated exposure times. Dominant emission occurs from 8-MNH-RF and 8-NH_2-RF. (b) Fluorescence detection at λ_{det} = 450 nm (dominant emission from 8-dimethylamino-lumichrome, 8-methylamino-lumichrome, and 8-amino-lumichrome).

RoF degradation was about the same as in the case of lower concentration (line-connected circles), but with time of exposure it became faster than at lower RoF concentration (shorter distance between RoF and 8-MNH-RF). The dash-dotted-line connected squares for RoF at 4 °C belong to 10 mM NaP_i at pH 10 (composition: 0.14 mM Na_3PO_4, 9.84 mM Na_2HPO_4, and 10 mM NaCl). The absorption changes were smaller than at pH 8 indicating a higher photo-stability. The concentration of $Na^{2+}HPO_4^{2-}$ in 10 mM pH 10 buffer (9.84 mM) is only slightly larger than at pH 8 (9.32 mM). The increased photo-stability seems to be caused by the higher pH. It should be noted that at pH 10 nearly half of the RoF molecules are in the anionic state ($pK_a = 10.2$ [17]).

In Fig. 6c, the photo-degradation of RoF in 10 mM NaP_i pH 8 buffer was studied for different excitation wavelengths (λ_{exc} = 425–503 nm, 532 nm, and 546 nm) at 4 °C. The absorption coefficient at λ_{pr} = 540 nm is plotted versus incident exposed energy density. The initial efficiency of photo-degradation was approximately the same in all three cases, but the speed-up of photo-degradation with exposed energy density was different. At λ_{exc} = 425–503 nm the light exposure excites both RoF and the primary photoproduct 8-MNH-RF, which enhances the photo-degradation of RoF. At λ_{exc} = 532 nm the photoproduct 8-MNH-RF is still slightly absorbing, and the photo-excited 8-MNH-RF enhances the photo-degradation of RoF. In the case of excitation at λ_{exc} = 546 nm, 8-MNH-RF is no longer absorbing, therefore no longer influenced the photo-degradation of RoF, and the quantum yield of photo-degradation of RoF remained constant independent of the exposed energy density.

In Fig. 9a, the initial quantum yield of photo-degradation, $\phi_{D,0}$, of RoF is depicted versus buffer concentration, C_b, for phosphate buffer at pH 8 and Tris–HCl buffer at pH 8 (excitation at 425–503 nm). One data point for phosphate buffer at pH 10 is included. The data point at $C_b = 0$ belongs to pure Millipore water. The measurements were carried out at 4 °C. The quantum yield of photo-degradation of RoF in Millipore water is $\phi_{D,0} = 9 \times 10^{-8}$. The photo-stability of RoF decreases with the buffer concentration for both phosphate buffer and Tris buffer. The photo-stability of RoF in the Tris buffer is roughly an order of magnitude higher than that in the phosphate buffer.

In Fig. 9b, the maximum quantum yield of photo-degradation, $\phi_{D,max}$, in the course of light exposure is plotted versus RoF concentration, C_0. Excitation occurred in the wavelength range 425–503 nm. With the exception of 47 μM RoF in pH 8 10 mM NaP_i buffer the samples were measured at 4 °C. The solid-line-connected circles belong to RoF in 10 mM NaP_i pH 8 buffer. At low dye concentration the photo-degradation is independent of concentration and it is $\phi_{D,max} = \phi_{D,0}$. In a medium dye concentration range the quantum yield of photo-degradation rises steeply with concentration. In the range of highest dye concentration, a linear rise of photo-degradation with dye concentration is observed. This behaviour will be interpreted below as diffusion controlled degradation of RoF by collision with photo-excited 8-MNH-RF or 8-NH_2-RF. The initial quantum yield of photo-degradation, $\phi_{D,0}$, was found to be independent of dye concentration within our experimental accuracy (no 8-MNH-RF or 8-NH_2-RF is present for photo-degradation enhancement).

The quantum yields of photo-degradation, $\phi_{D,max}$, of RoF in 10 mM NaP_i at pH 10 and of RoF in 100 mM NaP_i at pH 8 were measured only at one dye concentration. The efficiency of photo-degradation was higher at higher buffer concentration. It was lower at pH 10 than at pH 8.

In the case of RoF in pure Millipore water and in the case of Tris–HCl buffer, the RoF photo-degradation was only followed over the initial start phase of degradation (less than 10% of RoF degraded) because of the high photo-stability. The photo-degradation products are expected to be 8-MNH-RF and fully reduced roseoflavin (RoF_{red2}) as in the case of RoF in pH 8 NaP_i buffer because of observed remarkable fluorescence rise with exposure which agrees with 8-MNH-RF formation.

After long-time photo-excitation of RoF in phosphate buffer, a component with absorption out to 590 nm remained (Fig. 5). Its fluorescence quantum yield was measured by fluorescence excita-

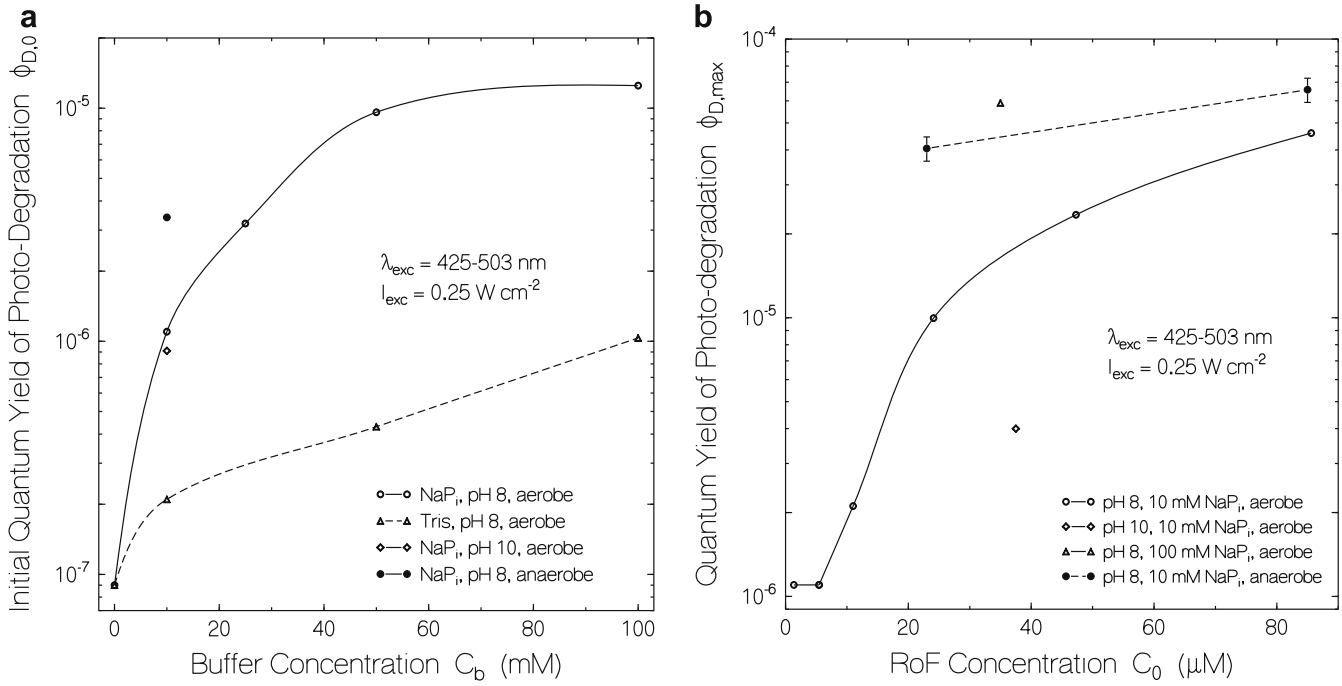

Fig. 9. (a) Dependence of initial quantum yield of photo-degradation, $\phi_{D,0}$, of RoF on buffer concentration, C_b. Excitation wavelength λ_{exc} = 425–503 nm, excitation intensity I_{exc} = 0.25 W cm^{-2}. The pH values and buffer compositions are indicated in the figure legend. (b) Dependence of maximum quantum yield of photo-degradation, $\phi_{D,max}$, of RoF on its initial concentration, C_0. Excitation wavelength λ_{exc} = 425–503 nm, excitation intensity I_{exc} = 0.25 W cm^{-2}. pH values and buffer compositions are indicated in the figure legend.

tion at 550 nm. A value of $\phi_F \approx 0.016$ was estimated. Its fluorescence decay was determined by picosecond laser pulse excitation at 527 nm (duration ≈ 6 ps) and streak-camera fluorescence detection (curves not shown). A bi-exponential fluorescence decay was found with a short component of lifetime $\tau_{F,1} = 15 \pm 5$ ps (integrated amount of $\phi_{F,1}/\phi_F = 0.25$) and a slow component of lifetime $\tau_{F,2} = 2.2 \pm 0.1$ ns (integrated amount of $\phi_{F,2}/\phi_F = 0.75$). The fast component has an approximate S_1–S_0 radiative lifetime of $\tau_{rad,1} = \tau_{F,1}/\phi_{F,1} \approx 4$ ns. It likely belongs to a quinonoid roseoflavin photoproduct (likely 8-MNH-1-methyl-quinone-riboflavin). The slow component has a radiative lifetime of $\tau_{rad,2} = \tau_{F,2}/\phi_{F,2} \approx 200$ ns. It may belong to fully reduced 8-amino-riboflavins.

A quantitative analysis of the fluorescence spectra in Fig. 7a and of the absorption coefficient spectra in Fig. 5b gives a fluorescence quantum yield of $\phi_F = 0.40 \pm 0.04$ for 8-MNH-RF in aqueous pH 8 10 mM NaP_i. Combined with the fluorescence lifetime of $\tau_F = 2.18 \pm 0.1$ ns for 8-MNH-RF (Fig. 4c) a radiative lifetime of $\tau_{rad} = \tau_F/\phi_F = 5.5 \pm 0.6$ ns (Eq. (2d)) and an S_0–S_1 absorption strength of $\bar{\sigma}_a = (2.6 \pm 0.3) \times 10^{-17}$ cm^2 (Eq. (1)) are calculated ($\bar{\lambda}_F = 577$ nm).

For RoF in pH 8 10 mM NaP_i buffer the photo-stability was also investigated under anaerobe sample conditions (de-aerating by Ar bubbling for 1 h). The de-aerated samples were photo-excited at $\lambda_{exc} = 425$–503 nm with an intensity of $I_{exc} = 0.25$ W cm^{-2}. The temperature was kept at 4 °C. The initial quantum yield of photo-degradation, $\phi_{D,0}$, increased roughly a factor of three compared to the aerobe sample. A data point is included in Fig. 9a. The maximum quantum yield of photo-degradation, $\phi_{D,max}$, during exposure also increased for the anaerobe samples compared to the aerobe samples. The result is included in Fig. 9b (two dashed-line connected dots). The increased photo-sensitizing of RoF degradation by 8-MNH-RF under anaerobe conditions will be explained below by an enlarging of the RoF and 8-MNH-RF triplet lifetime.

4. Discussion

Some determined parameters of RoF, and of the primary RoF photo-degradation product, 8-MNH-RF, in aqueous pH 8 10 mM NaP_i buffer are collected in Table 1.

The fluorescence behaviour of roseoflavin in aqueous solution and in organic solvents was investigated in [9,16]. The weak fluorescence efficiency was attributed to photo-induced twisted intra-molecular charge-transfer (TICT state formation) with non-radiative charge recombination. The same fluorescence behaviour was found here for roseoflavin in the investigated solvents (Millipore water, phosphate buffer solution, Tris–HCl buffer solution).

Table 1
Parameters of RoF, and 8-MNH-RF in aqueous pH 8 10 mM sodium phosphate buffer at room temperature under aerobe conditions.

Parameter	RoF	8-NMH-RF	Comments
$\lambda_{a,max}$ (nm)	504	488	Fig. 2
$\Delta\bar{\nu}_a$ (cm^{-1})	3200	2500	Fig. 2
$\sigma_{a,max}$ (cm^2)	1.33×10^{-16}	1.68×10^{-16}	Fig. 2
$\lambda_{F,max}$ (nm)	539	560	Figs. 3 and 7a
$\Delta\bar{\nu}_F$ (cm^{-1})	2860	2940	Figs. 3 and 7a
$\delta\bar{\nu}_{St}$ (cm^{-1})	1250	2890	$\delta\bar{\nu}_{St} = \lambda_{a,max}^{-1} - \lambda_{F,max}^{-1}$
$\bar{\nu}_{01}$ (cm^{-1})	19 180	19 300	$\bar{\nu}_{01} = (\lambda_{a,max}^{-1} + \lambda_{F,max}^{-1})/2$
ϕ_F	6.7×10^{-5}	≈0.4	Eqs. (2a)–(2c), Fig. 7a
τ_{rad} (ns)	6.5	5.5	Eq. (1)
$\tau_{F,1}$ (ps)	0.44	2180	Eq. (2d)
$\phi_{D,0}$	1.15×10^{-6}	$\approx 2 \times 10^{-5}$	Fig. 6a, Eq. (3)

Abbreviations. $\lambda_{a,max}$: Wavelength position of maximum S_0–S_1 absorption. $\Delta\bar{\nu}_a$: Spectral half-width (FWHM) of S_0–S_1 absorption band. $\sigma_{a,max}$ = absorption cross-section at $\lambda_{a,max}$. $\lambda_{F,max}$: Wavelength position of maximum fluorescence emission. $\Delta\bar{\nu}_F$: Spectral half-width (FWHM) of S_0–S_1 fluorescence band. $\delta\bar{\nu}_{St}$: Fluorescence Stokes shift. $\bar{\nu}_{01}$: Electronic S_0–S_1 transition wavenumber. ϕ_F: Intrinsic fluorescence quantum yield. τ_{rad}: S_1-state radiative lifetime. $\tau_{F,1}$: fluorescence lifetime (see text). $\phi_{D,0}$: Initial quantum yield of photo-degradation.

The photo-stability of roseoflavin in organic solvents has not yet been studied in detail [24]. A high photo-stability in neutral water was reported in [24]. Our own photo-degradation studies on RoF in pure Millipore water in this work give a quantum yield of photo-degradation of $\phi_{D,0} \approx 9.1 \times 10^{-8}$ (see above). The photolysis products of roseoflavin in alkaline and acidic aqueous solutions were identified in [24]: In 0.1 M NaOH RoF photo-degraded to 8-MNH-RF, while in 6 M HCl RoF photo-degraded to 7-methyl-8-dimethylamino-alloxazine (8-dimethylamino-lumicrome, 8-M2 N-LC).

Our studies on RoF in aqueous pH 8 phosphate buffer (phosphate composition 6.8% $Na^+H_2PO_4^-$ and 93.2% $Na_2^{2+}HPO_4^{2-}$) clearly show phosphate buffer catalysed photo-degradation (see Fig. 9a). In photolysis studies on riboflavin it was found a di-anionic catalysis of conversion of riboflavin to 2′,9-cyclo-dehydro-riboflavin by PO_4^{2-} and SO_4^{2-} [20] (peak absorption at 407 nm). We think that PO_4^{2-} also catalyses the photo-degradation of RoF, but resolvable formation of 2′,9-cyclo-dehydro-roseoflavin formation was not observed. Here, different 8-amino-flavin derivatives were formed as intermediates or final products during light exposure. Structural formulae of involved classes of 8-amino-flavin derivatives are shown in Fig. 1 [8-amino-isoalloxazines (flavins), 8-amino-alloxazines (lumichromes), 8-amino-quinone-flavins, fully reduced 8-amino-flavins)]. Possible constituents of the groups R_i are listed in the caption of Fig. 1.

Some enhancement of photo-degradation of RoF by the Tris–HCl buffer was also observed. Only the efficiency of enhancement was at least an order of magnitude reduced. The atomistic catalytic action of the phosphate buffer and Tris buffer on the photo-conversion of RoF is not yet known.

A proposed scheme of photo-degradation of RoF is described in the following:

The primary process of photo-degradation, where initially only RoF is present, is illustrated in Scheme 1. Light absorption excites RoF in the S_0 ground-state to the S_1-state in locally excited-state conformation $^1RoF^*_{LE}$. There occurs fast intra-molecular charge-transfer (ICT) to RoF^*_{CT}. The charge-transfer state returns to the ground-state by charge recombination (CR). During the lifetime of $^1RoF^*_{LE}$ there occurs some intersystem-crossing (ISC) to the triplet state $^3RoF^*$ (rate of intersystem-crossing $k_{ISC} \approx 1 \times 10^8$ s^{-1} [31–33]). The quantum yield of triplet formation is given by

$$\phi_T = k_{ISC}\tau_F, \tag{4}$$

which gives $\phi_T \approx 4.4 \times 10^{-5}$ for RoF in pH 8 10 mM NaP_i buffer ($\tau_F \approx 0.44$ ps). The lifetime τ_T of $^3RoF^*$ is estimated below to be $\tau_T \approx 4.5$ μs under our aerobic experimental conditions (under anaerobe condition a triplet lifetime of 36 μs was measured for 8-NH_2–RF in pH 7 phosphate buffer at 26 °C [34]). During the triplet-state lifetime degradation takes place. The initial quantum efficiency of degradation in the triplet state is given by

$$\phi_{D,0,T} = \frac{\phi_{D,0}}{\phi_T} \tag{5}$$

In the case of RoF in pH 8 10 mM NaP_i buffer under aerobe conditions, we estimate an efficiency of $\phi_{D,0,T} \approx 0.025$ ($\phi_{D,0} \approx 1.15 \times 10^{-6}$, $\phi_T \approx 4.4 \times 10^{-5}$) The catalytic effect of the phosphate buffer in the photo-degradation of RoF is active in the triplet state of RoF. Dominant primary photoproducts are 8-methylamino-riboflavin (8-MNH-RF, absorption maximum at 488 nm, fluorescence quantum yield of about 0.4) and fully reduced roseoflavin (RoF_{red2}). The 8-MNH-RF formation may proceed via methyl-nitrogen bond fissure at the dimethylamino group and

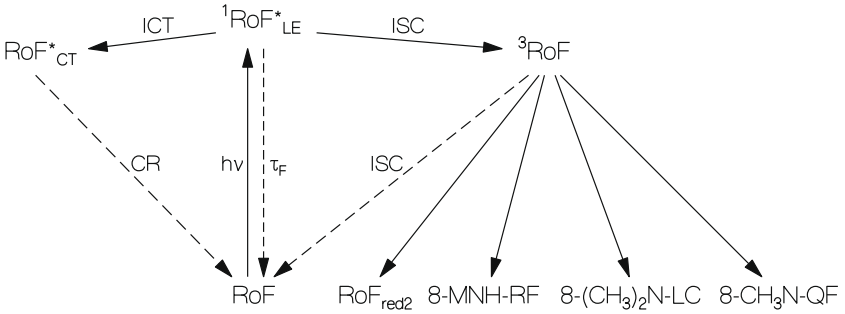

Scheme 1.

subsequent interaction of the radicals with the aqueous solution (catalytic action of phosphate and Tris buffer) giving a formal reaction according to

$$^3\text{RoF}^* + \text{HOH} \rightarrow \text{8-MN-RF}^{\cdot} + {}^{\cdot}\text{CH}_3 + \text{HOH} \rightarrow \text{8-MNH-RF} + \text{CH}_3\text{OH} \quad \text{(R1)}$$

The buffer catalysed reduction of RoF* to RoF$_{red2}$ may be due to intra-molecular photo-reduction (hydrogen abstraction at C2′ or C4′ position of ribityl part) [35] according to

$$^3\text{RoF}^* \rightarrow \text{RoF}_{red2} \quad \text{(R2a)}$$

where RoF$_{red2}$ = 8-M2N-10-C2′-keto-ribityl-1-H-5-H-isoalloxazine or 8-M2N-10-C4′-keto-ribityl-1-H-5-H-isoalloxazine. Or it may be due to intermolecular photo-reduction like

$$^3\text{RoF}^* + \text{HOH} \rightarrow \text{RoF}_{red2} \quad \text{(R2b)}$$

In this case, RoF$_{red2}$ is 1-OH-5-H-roseoflavin or 1-H-5-OH-roseoflavin. The formation of RoF$_{red2}$ is concluded from the reduced sample absorption (absorption of fully reduced flavin is small in blue and violet spectral part [36]). A minor conversion of excited RoF to 8-dimethylamino-lumichrome (splitting-off of ribityl part) according to [9]

$$^3\text{RoF}^* \rightarrow \text{8-M2N-LC} + \text{rybityl-ene} \quad \text{(R3)}$$

is indicated by the 450 nm fluorescence excitation spectra (Fig. 8b) and the 360 nm fluorescence emission spectra (Fig. 7b). Some excited RoF molecules seem to tautomerize to 8-amino-quinone-flavins according to

$$\text{RoF}^* \rightarrow \text{8-methylamino-1-methyl-quinone-flavin} \quad \text{(R4)}$$

(AQF formation). This formation is indicated by the build-up of an absorption band in the 520–600 nm range (Fig. 5a and b).

Without the presence of RoF, the photo-excitation of the strongly absorbing 8-MNH-RF (Fig. 2) causes degradation to a fully reduced amino-flavin (8-MNH-RF$_{red2}$), to 8-amino-riboflavin (8-NH$_2$-RF), and to 8-methylamino-lumichrome (8-MNH-LC) as is shown in Scheme 2. The photo-excitation of 8-MNH-RF forms singlet excited ^{1}8-MNH-RF* with a fluorescence lifetime of $\tau_F \approx 2.2$ ns. Intersystem-crossing from ^{1}8-MNH-RF* to ^{3}8-MNH-RF* takes place during this fluorescence lifetime. The quantum yield of triplet formation is estimated to be $\phi_T = k_{ISC}\tau_F \approx 0.22$ ($k_{isc} \approx 10^8$ s^{-1} used). The ^{3}8-MNH-RF* molecules dominantly return to the singlet ground-state by T_1–S_0 intersystem-crossing (triplet lifetime $\tau_T \approx 4.5$ μs under our aerobe conditions, see below). The quantum yield of photo-degradation of ^{3}8-MNH-RF* in pH 8 10 mM NaP$_i$ buffer is estimated to be $\phi_{D,T} = \phi_D/\phi_T \approx 10^{-4}$ ($\phi_D \approx 2 \times 10^{-5}$, see above). During the excited-state lifetime 8-MNH-RF molecules degrade to 8-amino-riboflavin by methyl-nitrogen bond fissure at the dimethylamino group in a formal (buffer catalized) reaction according to

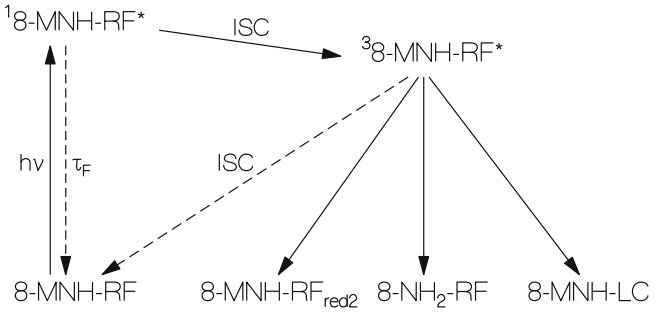

Scheme 2.

$$^3\text{8-MNH-RF}^* + \text{HOH} \rightarrow \text{8-NH-RF}^{\cdot} + {}^{\cdot}\text{CH}_3 + \text{HOH} \rightarrow \text{8-NH}_2\text{-RF} + \text{CH}_3\text{OH}. \quad \text{(R5)}$$

They degrade to fully reduced 8-MNH-RF in an intra-molecular reaction according to

$$^3\text{8-MNH-RF}^* \rightarrow \text{8-MNH-RF}_{red2,} \quad \text{(R6a)}$$

(8-MNH-RF$_{red2}$ = 8-MNH-10-C2′-keto-ribityl-1-H-5-H-isoalloxazine or 8-MNH-10-C4′-keto-ribityl-1-H-5-H-isoalloxazine) or an intermolecular reaction according to

$$^3\text{8-MNH-RF} + \text{HOH} \rightarrow \text{8-MNH-RF}_{red2,} \quad \text{(R6b)}$$

(8-MNH-RF$_{red2}$ = 8-MNH-1-OH-5-H-RF or 8-MNH-1-H-5-OH-RF) similar to the reactions R2a and R2b. Also some amino-lumichrome formation occurs according to

$$^3\text{8-MNH-RF}^* \rightarrow \text{8-MNH-LC} + \text{ribityl-ene}. \quad \text{(R7)}$$

The photo-excitation of 8-NH$_2$-RF (absorption cross-section spectrum included in Fig. 2) is thought to cause degradation according to Scheme 3. The fluorescence lifetime of 8-NH$_2$-RF is $\tau_F \approx 2.3$ ns [37]. The quantum yield of triplet formation is estimated to be $\phi_T \approx k_{ISC}\,\tau_F \approx 0.23$ using $k_{ISC} \approx 10^8$ s^{-1}. The photo-degradation of 8-NH$_2$-RF to 8-NH$_2$-RF$_{red2}$ is thought to be dominated by intra-molecular photo-reduction

$$^3\text{8-NH}_2\text{-RF}^* \rightarrow \text{8-NH}_2\text{-RF}_{red2,} \quad \text{(R8a)}$$

or intermolecular photo-reduction

$$^3\text{8-NH}_2\text{-RF}^* + \text{HOH} \rightarrow \text{8-NH}_2\text{-RF}_{red2,} \quad \text{(R8b)}$$

similar to (R2a) and (R2b) or (R6a) and (R6b). Also some lumichrome formation according to

$$^3\text{8-NH}_2\text{-RF}^* \rightarrow \text{8-NH}_2\text{-LC} + \text{ribityl-ene}, \quad \text{(R9)}$$

is expected to occur.

The proposed 8-MNH-RF sensitized RoF photo-degradation is illustrated in Scheme 4: The intermediate 8-MNH-RF strongly ab-

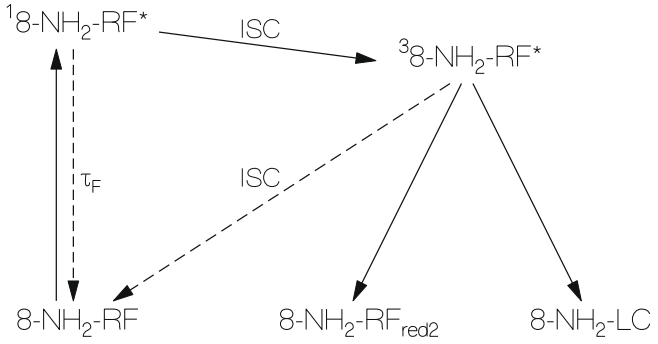

Scheme 3.

sorbs in the blue spectral range. Its photo-excitation causes intersystem-crossing to ^{3}8-MNH-RF* followed by excitation transfer (ET) [38–42] from ^{3}8-MNH-RF* to ^{1}RoF forming ^{1}8-MNH-RF and ^{3}RoF* according to

$$^3\text{8-MNH-RF}^* + {}^1\text{RoF} \rightarrow {}^1\text{8-MNH-RF} + {}^3\text{RoF}^*. \quad \text{(R10)}$$

The created triplet roseoflavin then degrades as described above by (R1), (R2a), (R2b), (R3), (R4). The excitation transfer from ^{3}8-MNH-RF* to ^{1}RoF with ^{1}8-MNH-RF and ^{3}RoF* formation may occur via iso-energetic (resonant) Dexter-type energy transfer [40–42] with subsequent vibronic relaxation as illustrated in Fig. 10a, or by combined exothermic reductive and oxidative (cross) electron transfers [38,39,42] as illustrated in Fig. 10b.

The 8-MNH-RF intermediate sensitizing of RoF degradation explains the speed-up of roseoflavin photo-degradation with exposure time: the more 8-MNH-RF is present the more efficient is the RoF photo-degradation. It explains the wavelength dependence of the RoF photo-degradation: when the excitation occurred in the long-wavelength transparency region of 8-MNH-RF, then the formed 8-MNH-RF could not be excited and the sensitization process (R10) could not occur. The 8-MNH-RF sensitized RoF photo-degradation also explains the decreasing sensitizing efficiency of RoF photo-degradation with sample dilution: Dexter-type excitation transfer and combined reductive and oxidative electron transfer occur only when a ^{3}8-MNH-RF* molecule collides with a ^{1}RoF molecule. This means that within the triplet lifetime τ_T of 8-MNH-RF the molecules RoF and ^{3}8-MNH-RF* have to collide by diffusion motion.

The collision condition for sensitized photo-degradation of RoF may be applied to estimate the triplet lifetime of 8-MNH-RF. The average (centre–centre) distance a_{cc} between two molecules in solution of number density N_m is $a_{cc} \approx N_m^{-1/3}$. This distance has to be overcome by the diffusion length ℓ_d within the triplet-state lifetime τ_T. ℓ_d is given by [43]

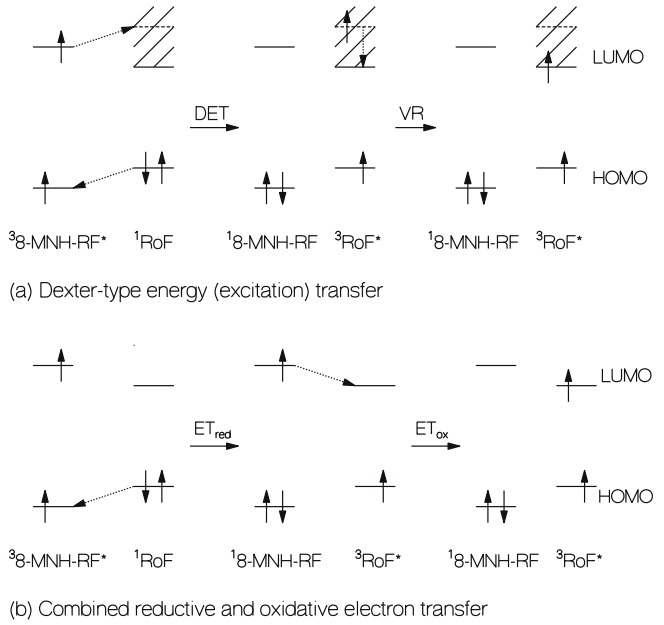

Fig. 10. Illustration of singlet–triplet inter-change (a) by Dexter-type energy (excitation) transfer, and (b) by combined reductive and oxidative (cross) electron transfer. DET = Dexter energy transfer. VR = vibrational intra-band relaxation. ET_{red} = reductive electron transfer. ET_{ox} = oxidative electron transfer. Hatched area indicates vibronic structure of first excited band. Lower levels represent HOMO states, and upper levels represent LUMO states (HOMO = highest occupied molecular orbital, LUMO = lowest unoccupied molecular orbital).

$$\ell_d = (2D\tau_T)^{1/2}, \quad (6)$$

where D is the diffusion constant. D may be obtained from the Stokes–Einstein equation [43],

$$D = \frac{k_B\vartheta}{6\pi\eta a_m}, \quad (7)$$

where k_B is the Boltzmann constant, ϑ is the temperature, η is the viscosity of the solvent, and a_m is the (solute) molecule radius. Using experimental parameters of ϑ = 277 K, $\eta = 1.003 \times 10^{-3}$ Pa s (solvent water), and a_m = 0.633 nm (average molecule radius of RoF) a diffusion constant of $D = 3.38 \times 10^{-6}$ cm^{2}s^{-1} is calculated. In Fig. 9b, a steep rise in RoF photo-degradation sets in at a critical molecule concentration of $C_{m,cr} \approx 10^{-5}$ mol dm^{-3} corresponding to a critical dye number density of $N_{m,cr} = C_{m,cr}N_A/1000 \approx 6 \times 10^{15}$ cm^{-3} (N_A is Avogadro constant) and a critical molecule distance of $a_{cc,cr} = N_{m,cr}^{-1/3} \approx 55$ nm. Setting $\ell_d = a_{cc,cr}$ in Eq. (6) we estimate a triplet-state lifetime of $\tau_T \approx 4.5$ μs.

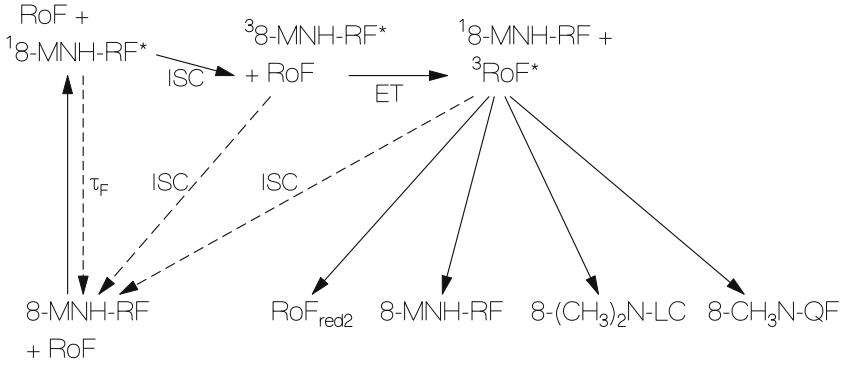

Scheme 4.

Under anaerobe conditions the initial quantum yield of photo-degradation, $\phi_{D,0}$, increased likely because of longer triplet-state lifetime (longer $^3RoF^*$ lifetime enables longer catalytic buffer interaction time for degradation). Also the maximum quantum yield of 8-MNH-RF sensitized photo-degradation of RoF, $\phi_{D,max}$, increased since the triplet-state lifetimes of 8-MNH-RF and RoF increased (longer time for collision excitation transfer from ^{3}8-MNH-RF* to ^{1}RoF, and longer lifetime of formed $^3RoF^*$). The photo-degradation sensitizing enhancement under anaerobe conditions excludes the involvement of singlet excited molecular oxygen in the photo-degradation, since $^1O_2$ may be only formed by excited-state triplet flavin – ground-state triplet oxygen annihilation according to $^3\text{flavin}^* + {}^3O_2 \rightarrow {}^1\text{flavin} + {}^1O_2^*$ under aerobe conditions [38,39]. In the case of singlet oxygen involvement, the opposite behaviour should have been observed (i.e. higher photo-degradation under aerobe conditions should have occurred).

5. Conclusions

Roseoflavin in aqueous solution was found to have very low fluorescence quantum yield and sub-picoseond fluorescence lifetime at room-temperature due to photo-induced intra-molecular charge-transfer [9,16].

The photo-stability of roseoflavin was studied in un-buffered Millipore water, in pH 8 and pH 10 phosphate buffer, and in pH 8 Tris–HCl buffer. The highest photo-stability was observed for Millipore water and the lowest photo-stability was found in phosphate buffer. The photo-degradation of roseoflavin is thought to occur dominantly in the triplet state. The primary photoproduct of roseoflavin photo-degradation, 8-methylamino-riboflavin, exhibits reasonably high fluorescence quantum yield and fluorescence lifetime. It strongly enhances the degradation of roseoflavin by photo-induced excitation transfer (Dexter-type and combined HOMO and LUMO electron transfer) from triplet 8-methylamino-riboflavin to singlet ground-state roseoflavin with subsequent degradation of the formed triplet roseoflavin.

Acknowledgements

The work was supported by the Deutsche Forschungsgemeinschaft (DFG): GK640 (A.P.), FOR526 (A.P., P.H.), SFB 498 (P.H.) and the Cluster of Excellence "Unifying Concepts in Catalysis" (P.H.). A.P. is grateful to Profs. F.J. Gießibl and J. Repp for their kind hospitality.

References

[1] K. Matsui, S. Kasai, in: F. Müller (Ed.), Chemistry and Biochemistry of Flavoenzymes, vol. 1, CRC Press, Boca Raton, FL, 1991, p. 105.
[2] W. Friedrich, Vitamins, Walter de Gruyter, Berlin, 1988. p. 445.
[3] S. Otani, in: T.P. Singer (Ed.), Flavins and Flavoproteins, Elsevier, Amsterdam, 1976, p. 323.
[4] S. Kasai, S. Yamanaka, H.-C. Wang, K. Matsui, J. Nutr. Sci. Vitaminol. 25 (1979) 289.
[5] T. Mathes, C. Vogl, J. Stolz, P. Hegemann, J. Mol. Biol. 385 (2009) 1511.
[6] S. Otani, S. Kasai, K. Matsui, Methods Enzymol. 66 (1980) 235.
[7] K. Yorita, H. Misaki, B.A. Palfey, V. Massey, PNAS 97 (2000) 2480.
[8] R. Flores, A. Dederichs, E. Cerdá-Olmedo, R. Hertel, Plant Biol. 1 (1999) 645.
[9] P. Zirak, A. Penzkofer, T. Mathes, P. Hegemann, J. Photochem. Photobiol. B 97 (2009) 61.
[10] M.K. Otto, M. Jayaram, R.M. Hamilton, M. Delbrück, PNAS 78 (1981) 266.
[11] S. Kasai, R. Miura, K. Matsui, Bull. Chem. Soc. Jpn. 48 (1975) 2877.
[12] K. Shiga, K. Horuke, Y. Nishina, S. Otani, H. Watari, T. Yamano, Biochemistry 85 (1979) 931.
[13] V.M. Berezovskii, A.I. Stepanov, N.A. Polyakova, L.S. Tul'chinskaya, A.Ya. Kukanova, Bioorg. Chem. 3 (1977) 393.
[14] S. Shinkai, K. Kameoka, N. Honda, K. Ueda, O. Manabe, J. Lindsey, Bioorg. Chem. 14 (1986) 119.
[15] K. Matsui, N. Juri, Y. Kubo, S. Kasai, J. Biochem. 86 (1979) 167.
[16] P. Zirak, A. Penzkofer, T. Mathes, P. Hegemann, Chem. Phys. 358 (2009) 111.
[17] P.-S. Song, E.B. Walker, R.D. Vierstra, K.L. Poff, Photochem. Photobiol. 32 (1980) 393.
[18] B.J. Fritz, S. Kasai, K. Matsui, Photochem. Photobiol. 45 (1987) 113.
[19] B. Holmström, Arkiv. Kemi. 22 (1964) 281.
[20] M. Schuman Jorns, G. Schöllnhammer, P. Hemmerich, Eur. J. Biochem. 57 (1975) 35.
[21] I. Ahmad, Q. Fasihullah, F.H.M. Vaid, J. Photochem. Photobiol. B 75 (2004) 13.
[22] I. Ahmad, Q. Fasihullah, F.H.M. Vaid, J. Photochem. Photobiol. B 78 (2005) 229.
[23] W. Scheidler, A. Penzkofer, Opt. Commun. 80 (1990) 127.
[24] K. Matsui, S. Kasai, in: T.P. Singer (Ed.), Flavins and Flavoproteins, Elsevier, Amsterdam, 1976, p. 328.
[25] P. Drössler, W. Holzer, A. Penzkofer, P. Hegemann, Chem. Phys. 282 (2002) 429.
[26] S.J. Strickler, R.A. Berg, J. Chem. Phys. 37 (1962) 814.
[27] J.B. Birks, D.J. Dyson, Proc. Roy. Soc. Lond. Ser. A 275 (1963) 135.
[28] A.V. Deshpande, A. Beidoun, A. Penzkofer, G. Wagenblast, Chem. Phys. 142 (1990) 123.
[29] S.I. Vavilov, Z. Phys. 42 (1927) 311.
[30] G.N. Lewis, M. Kasha, J. Am. Chem. Soc. 66 (1944) 2100.
[31] N.J. Chacon, J. McLearie, R.S. Sinclair, Photochem. Photobiol. 47 (1988) 647.
[32] A. Losi, E. Polverini, B. Quest, W. Gärtner, Biophys. J. 82 (2002) 2627.
[33] S.D.M. Islam, A. Penzkofer, P. Hegemann, Chem. Phys. 291 (2003) 97.
[34] B.J. Fritz, K. Matsui, S. Kasai, A. Yoshimura, Photochem. Photobiol. 45 (1987) 539.
[35] W.L. Cairns, D.E. Metzler, J. Am. Chem. Soc. 93 (1971) 2772.
[36] F. Müller, S. Ghisla, A. Bacher, in: O. Isler, G. Brubacher, S. Ghisla, K. Kräutler (Eds.), Vitamine II, Thieme Verlag, Stuttgart, 1988, p. 50.
[37] A. Tyagi, P. Zirak, A. Penzkofer, T. Mathes, P. Hegemann, M. Mack, S. Ghisla, Chem. Phys. 364 (2009) 19.
[38] B. Valeur, Molecular Fluorescence: Principles and Applications, Wiley–VCH, Weinheim, 2002.
[39] N.J. Turro, V. Ramamurthy, J.C. Scaiano, Principles of Molecular Photochemistry: An Introduction, University Science Books, Sausalito, CA, 2009.
[40] D.L. Dexter, J. Chem. Phys. 21 (1953) 836.
[41] S. Speiser, Chem. Rev. 96 (1996) 1953.
[42] J. Shirdel, A. Penzkofer, R. Procházka, Z. Shen, J. Daub, Chem. Phys. 336 (2007) 1.
[43] P. Atkins, J. de Paula, Atkin's Physical Chemistry, eighth ed., Oxford University Press, Oxford, 2006.